Brownian Dynamics Simulations of Dendrimers under Shear Flow

Alexey V. Lyulin,† Geoffrey R. Davies, and David B. Adolf*

Interdisciplinary Research Centre in Polymer Science and Technology, University of Leeds, Leeds LS2 9JT, U.K.

Received December 21, 1999; Revised Manuscript Received March 1, 2000

ABSTRACT: Brownian dynamics simulations of perfect dendrimers up to the sixth generation have been performed under the influence of simple shear flow. Hydrodynamic and excluded volume interactions have been taken into account explicitly. The onset of shear-thinning is observed to occur at lower shear rates for larger dendrimers (i.e. more generations). As the generation increases, the zero shear rate intrinsic viscosity reaches a maximum and begins to fall. The radius of gyration, the hydrodynamic radius, the translational mobility, and radial density profiles including the location of the terminal groups are also reported.

I. Introduction

With the increasing ability to synthesize perfectly branched macromolecules (i.e. dendrimers) over the last two decades[1−3] has come a corresponding increase in efforts to understand their solution and bulk behavior. Relative to linear polymer chains with the same molecular mass, dendrimers possess good solubility and a decreased melt viscosity but poor mechanical properties due to low levels of crystallinity and interchain entanglements arising from their highly branched topology.[4,5]

Theoretical studies of de Gennes and Hervet[6] have focused on a mean-field model where it is assumed that all the segments belonging to a given generation lie in a concentric shell about a central core. However, efforts of Naylor et al.[7] based on molecular dynamics simulations and molecular mechanics calculations of dendrimers up to generation 7 have revealed open structures rather than a concentric shell assembly. Lescanec and Muthukumar[8] used an off-lattice kinetic growth algorithm to build dendrimers and found a density profile that decreases monotonically outward from the center of the molecule. The dendrimers simulated by Mansfield and Klushin[9] using Monte Carlo (MC) techniques revealed minima in the density profiles of the higher generation dendrimers studied. These findings were confirmed later by the MC simulations of Lue and Prausnitz.[10] Molecular dynamics simulations of dendrimers in solution[11] and within the glassy state[12] have been performed recently by Murat and Grest in addition to Mazo et al., correspondingly. Murat and Grest treated the solvent as a continuum and varied its quality by changing the energetic parameter of the Lennard−Jones (LJ) interactions between different monomers. The simulations did not take hydrodynamic interactions (HI) into account and were analyzed primarily in termsof properties such as the radius of gyration and the radial distribution function of monomers.

A very interesting feature of dendrimers is the experimentally observed relationship between their intrinsic viscosity (IV, $[\eta]$) and their molecular weight. Intrinsic viscosity is a measure of a polymer's ability to increase the viscosity of a solvent. log−log plots of a dendrimer's IV vs molecular weight increases until, at a critical generation, a maximum is observed followed by a steady fall in IV. In contrast to dendrimers, linear polymers obey the Mark−Houwink equation

$$[\eta] = KM^a \tag{1}$$

where K and a are constants for a given polymer/solvent/temperature system indicating a steady increase of IV with increasing molecular weight. Recent experiments by Okumoto et al.[13] show that eq 1 is valid also for star polymers in a Θ-solution with the same constant a but lower K. Okumoto et al. also show that intrinsic viscosity $[\eta]$ lowers with increasing arm number. In the case of dendrimers Mansfield and Klushin[14] followed a variational approach due to Fixman[15] to show that the IV goes through a maximum no earlier than the fourth generation. The IV of dendrimers calculated from the hydrodynamic tensor approach of Aerts[16] and from the radius of gyration by Widmann and Davies[17] also exhibit maxima. However, Cai and Chen[18] found that a more accurate treatment of the Mansfield−Klushin theory does not yield the anticipated maxima and proposed a new model in which the characteristic length of the excluded volume interactions is smaller than that for hydrodynamic interactions. They have shown that hydrodynamic interactions play a very important role and increasing the strength of HI leads to a more pronounced maximum on the dependence of IV on generation number.

Experimentally speaking, a recent rheological study of polyamidoamine (PAMAM) solutions using PAMAM dendrimers up to the seventh generation have been performed under the influence of steady shear flow by Tomalia et al.[19] It was found that these dendrimer solutions exhibit Newtonian flow behavior as manifested by the direct proportionality of shear stress to shear rate over the entire ranges studied.

In the present paper, Brownian dynamics (BD) is used to simulate the intrinsic viscosity and various statistical properties of dendrimers under the influence of shear flow. This method allows the intrinsic viscosity of a very dilute solution to be simulated over a broad range of shear rate. Hydrodynamic and excluded volume interactions are taken into account explicitly. In section II, the

* To whom correspondence should be addressed.
† On leave from the Institute of Macromolecular Compounds, Russian Academy of Sciences, 199004 St. Petersburg, Russia.

10.1021/ma992128a CCC: $19.00
Published on Web 04/14/2000

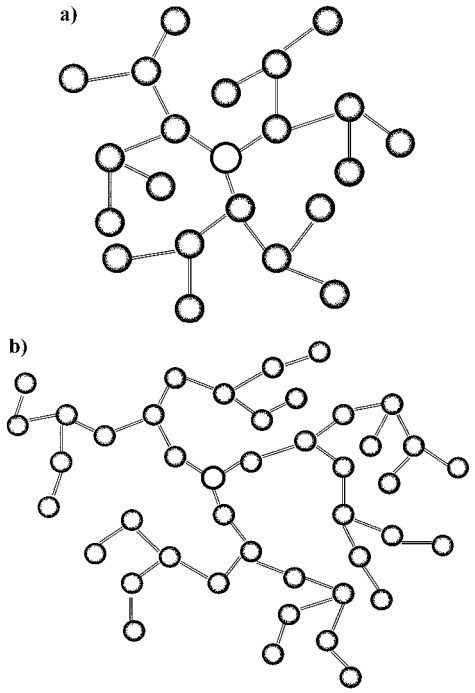

Figure 1. Simulated dendritic polymers: with (a) every bead branched (model A) and (b) every other bead branched (model B). Three generations are shown for each model and the trifunctional core is shown as a white sphere. Within these figures, the radius of the monomer unit is equal to 0.257*l* where *l* is a bond length.

model and details of the simulation algorithm are explained. The results are presented in section III and the main conclusions are summarized in section IV.

II. Simulation Models and Algorithm

Brownian dynamics simulations in the presence of shear flow of dendrimers with branching at every bead (model A) or branching at every other bead (model B) have been performed. These models are depicted in parts a and b of Figure 1, respectively.

Beads within both models possess a friction coefficient ζ and are connected by rigid rods of length l. The total number of generations for a given dendrimer is denoted by g where a $g = 0$ dendrimer contains a central core with three rigid bonds each connected to one (model A) or two (model B) beads, respectively. Up to the $g = 6$ generation for model A and up to the $g = 5$ generation for model B are simulated. Torsional and valence angle potentials are not employed, and the Ermak−McCammon[20] equation of motion is used where each integration step is calculated according to

$$\vec{r}_i = \vec{r}_i^{\,0} + \Delta t/kT\sum_j \mathbf{D}_{ij}^0\cdot\vec{F}_j^0 + \vec{v}_i^{\,0}\cdot\Delta t + \vec{\Phi}_i^0(\Delta t) \qquad i = 0, ..., N \quad (2)$$

$\vec{r}_i^{\,0}$ is the position vector for bead i before a Brownian dynamics step, Δt, where the core is considered when $i = 0$. k is Boltzmann's constant, and T is the simulation temperature. $\mathbf{D}_{ij}^0$ is the diffusion tensor and $\vec{v}_i^{\,0}$ is the velocity of the solvent at the position of bead i where for steady shear flow $v_{i,x}^0 = y_i^0\dot{\gamma}$, $v_{i,y}^0 = v_{i,z}^0 = 0$. The solvent is represented as a structureless continuum with chain-solvent collisions mimicked by the vector $\vec{\Phi}_i^0$ which has a zero mean and a variance-covariance matrix given by

$$\langle\vec{\Phi}_i^0(\Delta t)\vec{\Phi}_j^0(\Delta t)\rangle = 2\Delta t\mathbf{D}_{ij}^0 \quad (3)$$

When hydrodynamic interactions are neglected

$$D_{ii}^{(\alpha\beta)0} = (kT/\zeta)\delta_{\alpha\beta} \quad i = 0, ..., N \quad (4a)$$

$$D_{ij}^{(\alpha\beta)0} = 0 \quad \text{for } i \neq j = 0, ..., N \quad (4b)$$

where α and β both represent the x, y, or z components and $\delta_{\alpha\beta}$ is a Kronecker symbol. $\vec{F}_j^0$ in eq 2 is given by

$$\vec{F}_j^0 = -\sum_{k=1}^{N}\lambda_k\left(\frac{\partial\sigma_k}{\partial\vec{r}_j}\right)_{r^0} - \partial U_{LJ}/\partial\vec{r}_j^{\,0} \quad (5)$$

where σ_k is an equation of rigid constraint for the kth bond and λ_k is the corresponding Lagrange multiplier. The SHAKE algorithm[21] with a relative tolerance of 2×10^{-6} is used to maintain a fixed bond length. A Lennard−Jones potential, U_{LJ}, is invoked

$$U_{LJ} = \sum_{ij} 4\epsilon\left(\left(\frac{\sigma}{r_{ij}}\right)^{12} - \left(\frac{\sigma}{r_{ij}}\right)^{6}\right) \quad (6)$$

between all nonbonded beads i and j with a cutoff distance, r_{cutoff}, of 2.5σ. The parameters $\sigma = 0.8l$ and $\epsilon = 0.3kT$ are used as proposed by de la Torre and coworkers[22] to correctly reproduce the molecular-weight dependence of the average square end-to-end distance, $\langle R^2\rangle$, of a linear chain in a Θ-solution. HI are represented rigorously by means of the Rotne−Prager−Yamakawa interaction tensor.[23] The diagonal elements of the diffusion tensor $\mathbf{D}_{ii}$ are given by eq 4a and one has

$$D_{ij}^{\alpha\beta} = h^*(\pi/3)^{1/2}(3kT/4\zeta)(l/R_{ij})\left[\left(\delta_{\alpha\beta} + \frac{R_{ij}^\alpha R_{ij}^\beta}{R_{ij}^{\,2}}\right) + \frac{2a^2}{3R_{ij}^{\,2}}\left(\delta_{\alpha\beta} - \frac{3R_{ij}^\alpha R_{ij}^\beta}{R_{ij}^{\,2}}\right)\right] \quad (7a)$$

where R_{ij} is the separation between beads i and j each with Stokes' hydrodynamic radius a for nonoverlapping beads ($R_{ij} = |\vec{R}_{ij}| = |\vec{r}_i - \vec{r}_j| \geq 2a$). The strength of the HI effects is set by the parameter $h^* = (3/\pi)^{1/2}a/l = (3/\pi)^{1/2}\zeta/(6\pi\eta_s l)$ where η_s represents the solvent viscosity. Two values of h^*, $h^* = 0.25$ and $h^* = 0.44$, are used which corresponds to the hydrodynamic radius $a = 0.257l$ and $a = 0.45l$. If the beads are allowed to overlap ($R_{ij} < 2a$) eq 7a is rewritten as[23]

$$D_{ij}^{\alpha\beta} = (kT/\zeta)\left[\left(1 - \frac{9R_{ij}}{32a}\right)\delta_{\alpha\beta} + \left(\frac{3}{32a}\right)\frac{R_{ij}^\alpha R_{ij}^\beta}{R_{ij}}\right] \quad (7b)$$

In this paper, dimensionless quantities are represented by an asterisk where length (l), energy (kT), and translational friction $\zeta = 6\pi\eta_s a$ are set to unity. It follows that time is reduced by $\zeta l^2/kT$; and shear rate by $kT/\zeta l^2$. Dimensionless shear rates ranging from 0 to 10^2 are covered in this investigation. A dimensionless time step between $\Delta t = 1 \times 10^{-3}$ and 1×10^{-4} is used which decreases with increasing shear rate. The mag-

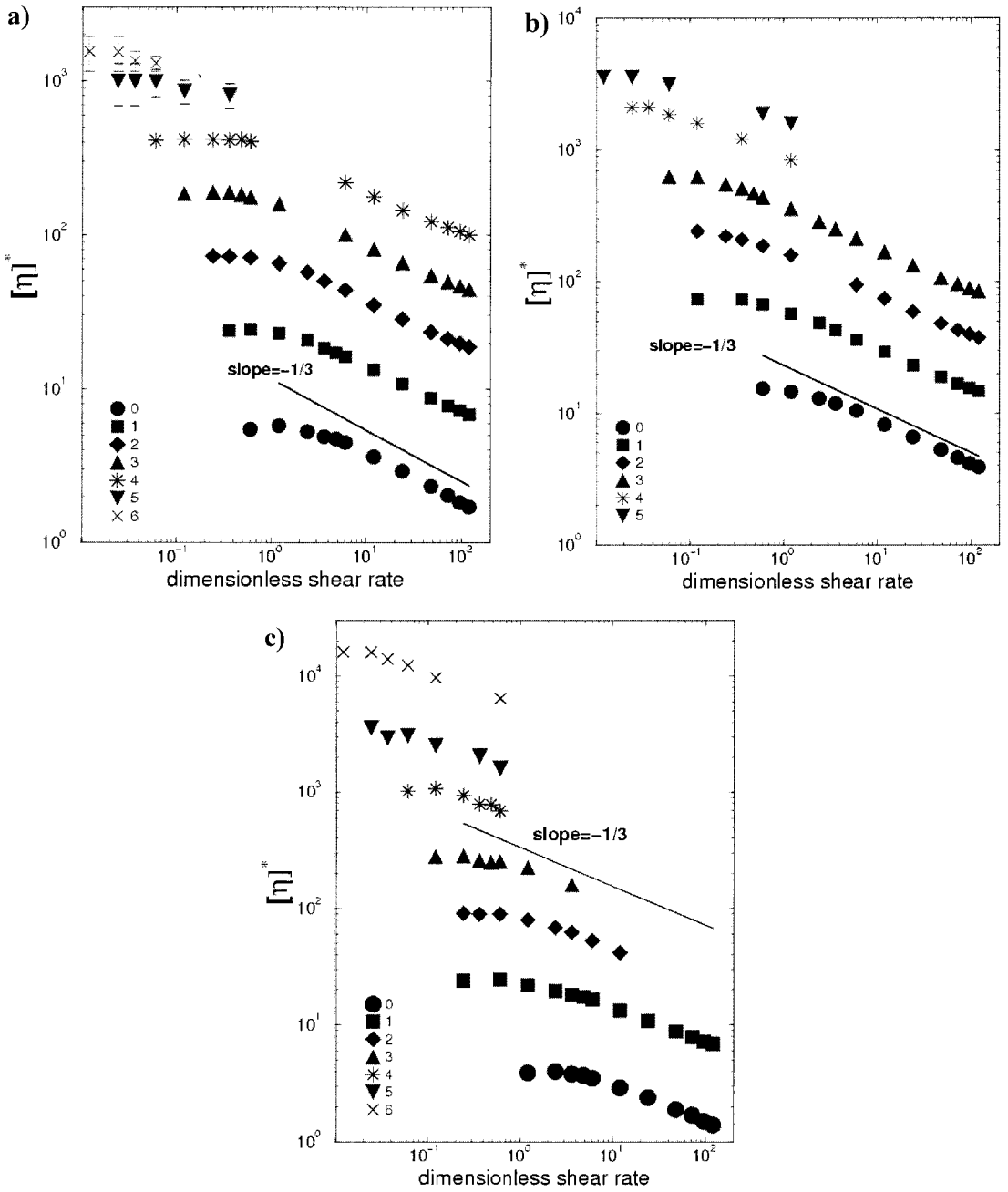

Figure 2. Dimensionless shear rate dependence of the dimensionless intrinsic viscosity for (a) a model A and (b) a model B dendrimer with the number of generations, g, ranging from 0 to 6 performed in the presence of hydrodynamic interactions ($h^* = 0.25$). For each generation a shear-thinning effect is observed. The onset of shear-thinning starts at smaller shear rates when increasing the size of the dendrimer for both models. Part c depicts results from a simulation of model A dendrimers performed without hydrodynamic interactions ($h^* = 0$). In all cases the limiting slope when $\dot{\gamma}^* \gg 1$ is very close to $-1/3$.

nitude of the time step is chosen so that the maximum displacement of a bead is less than 10% of the average bond length.

A procedure proposed by Murat and Grest[11] is used to generate the initial configurations up to $g = 6$. The generation $g = 0$ of the dendrimer is built attaching $b = 3$ chains of $n = 1$ (model A) or $n = 2$ (model B) monomers onto the core at three randomly chosen points. Each sphere of diameter σ is joined to a similar sphere through rigid bonds of length l. The next generation is built by adding $b - 1$ chains to each of the free ends of the previous generation. The distance between an added monomer and all other monomers is constrained to be larger than some distance $r_{min} = 0.8\sigma$. Bead overlaps are not allowed and if a monomer cannot be inserted after a reasonable number of trials (i.e., 500−600) the whole dendrimer is discarded and the procedure of growth is started from the beginning.

After generation of its initial configuration, the dendrimer is allowed to equilibrate for 100 000 to 500 000 time steps depending on the dendrimer size and magnitude of the shear rate. The attainment of a steady-state is monitored through the radius of gyration, R_g, and the components of the inertia tensor, $\boldsymbol{T}$. Following equilibration, production runs are performed consisting of an additional 400 000 to 3 000 000 time steps, again depending on the size of the system and magnitude of the shear rate. The normalized time autocorrelation

function of the squared radius of gyration is calculated according to

$$C_{R_g}(t) = \frac{\langle (R_g^2(0) R_g^2(t)) \rangle - \langle R_g^2 \rangle^2}{\langle R_g^4 \rangle - \langle R_g^2 \rangle^2} \tag{8}$$

A correlation time, t_{R_g}, is defined as the value of t where $C_{R_g}(t_{R_g}) = e^{-1}$. This correlation time decreases as the magnitude of shear flow increases and is less than 3−4 dimensionless time units in magnitude. The total length of the runs is equal to $50-100 t_{R_g}$.

The dimensionless intrinsic viscosity is calculated according to

$$[\eta]^* = \frac{(\eta - \eta_s)}{nkT\lambda} \tag{9a}$$

where the shear viscosity, η, is calculated through the nondiagonal component of the shear stress as

$$\eta = -\frac{\tau_{xy}}{\dot{\gamma}} \tag{9b}$$

The characteristic time, λ, (i.e., the characteristic time of orientational diffusion of a single monomer) is given as $\zeta l^2/12kT$ and n is the number density of dendrimers. In standard rheological experiments the intrinsic viscosity is related not to a number density of the polymer chains as used in eq 9a but rather to the concentration of chain monomers. For this reason, the normalized quantity $[\tilde{\eta}]_0 = [\eta]_0^*/N$ is also calculated where N is the total number of beads in the dendrimer. Other details of the simulation procedure are found within a previous publication.[24]

The following sections investigate the dependence of the simulated intrinsic viscosity and radius of gyration of dendrimers on the generation number, the molecular weight, and the magnitude of the shear flow. Comparisons are also made with similar findings for linear chains. The influence of the HI on the simulated properties is also reported in addition to radial density profiles and the translational mobility of the dendrimers' centers of mass. Note that error bars for all plotted data points are smaller than the size of the symbols used within the figures unless otherwise indicated.

III. Results and Discussion

A. Intrinsic Viscosity. Parts a−c of Figure 2 illustrate the shear thinning of the simulated intrinsic viscosity for model A dendrimers and model B dendrimers, respectively. Parts a and b of Figure 2 are produced from simulations which employ hydrodynamic interactions. No such interactions are used to generate the data plotted in Figure 2c.

At low shear rates, a Newtonian plateau in the intrinsic viscosity is observed with the onset of shear-thinning occurring at smaller shear rates as the size of the dendrimer increases. This effect is also seen for linear chains[24] but starts at higher shear rates as compared with linear analogues of the same molecular weight. To appreciate the rates required to shear thin model A and model B dendrimers, consider the $g = 4$ dendrimer in Figure 2a where the intrinsic viscosity begins to decrease at $\dot{\gamma}^* \sim 1$. A solvent viscosity of one centipoise, a bond length $l = 1.54$ Å and a temperature

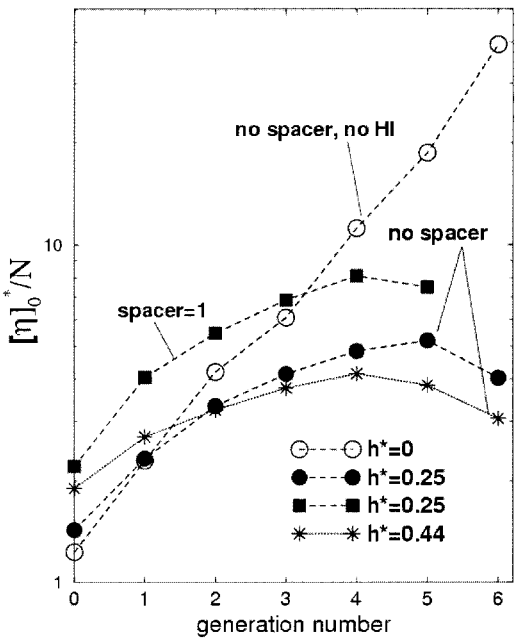

Figure 3. Normalized dimensionless zero-shear rate intrinsic viscosity as a function of generation number: free-draining dendrimer without spacers (model A without HI), open spheres; model A with different values of parameter h^* of HI, closed spheres and asterisks; dendrimer with HI and spacers (model B), closed squares. All nondraining models reveal a pronounced maximum.

$T \sim 300$ K affords a characteristic time on the order of 10^{-11} s and a shear rate of 10^{11} s^{-1}.

Parts a and b of Figure 2 reveal that at $\dot{\gamma}^* \gg 1$ the intrinsic viscosity of both model dendrimers scales as $[\eta]^* \sim \dot{\gamma}^{*\alpha}$ where α is found to be close to $-1/3$. This scaling seems to be independent of branching since the same behavior is found for free-draining and nondraining linear chains with rigid valence bonds.[24] Figure 2c reveals additional evidence that this scaling is not dependent on the presence of hydrodynamic interactions. The onset of shear-thinning starts at higher magnitudes of shear rate as compared to the nondraining case (cf. Figure 2a,b), but the asymptotic slope is again very close to $-1/3$.

For free-draining linear chains (i.e., Rouse model) $[\tilde{\eta}]_0 \sim N^{2\nu} \sim \langle R^2 \rangle$ where ν is the Flory exponent and $\langle R^2 \rangle$ is the mean-squared size (end-to-end distance or radius of gyration) of the chain.[25] For linear chains under Θ-conditions, $\nu = 1/2$ indicating that $[\tilde{\eta}]_0$ scales with the first power of molecular weight. For nondraining linear chains (i.e., Zimm model[25]) $[\tilde{\eta}]_0 \sim \langle R^3 \rangle / N$. The maximum in the dependence of $[\tilde{\eta}]_0$ vs molecular weight can be expected when the average volume of the polymer chain starts to increase slower than its molecular weight, which is typically true for dendrimers at high generations. $[\tilde{\eta}]_0$ is plotted in Figure 3 for model A and model B dendrimers where zero-shear intrinsic viscosities are deduced by extrapolating the curves found in parts a−c of Figure 2 to zero shear rate.

The open circles indicate a steadily increasing, nearly linear scaling of $[\tilde{\eta}]_0$ on generation number for free-draining dendrimers where hydrodynamic interactions are neglected. The filled circles and squares reveal this is not the case for the nondraining dendrimers, where hydrodynamic interactions are taken into account. The nondraining data reveal a pronounced maximum in $[\tilde{\eta}]_0$ around $g = 4-5$. This fact is also observed experimentally for PAMAM dendrimers.[26]

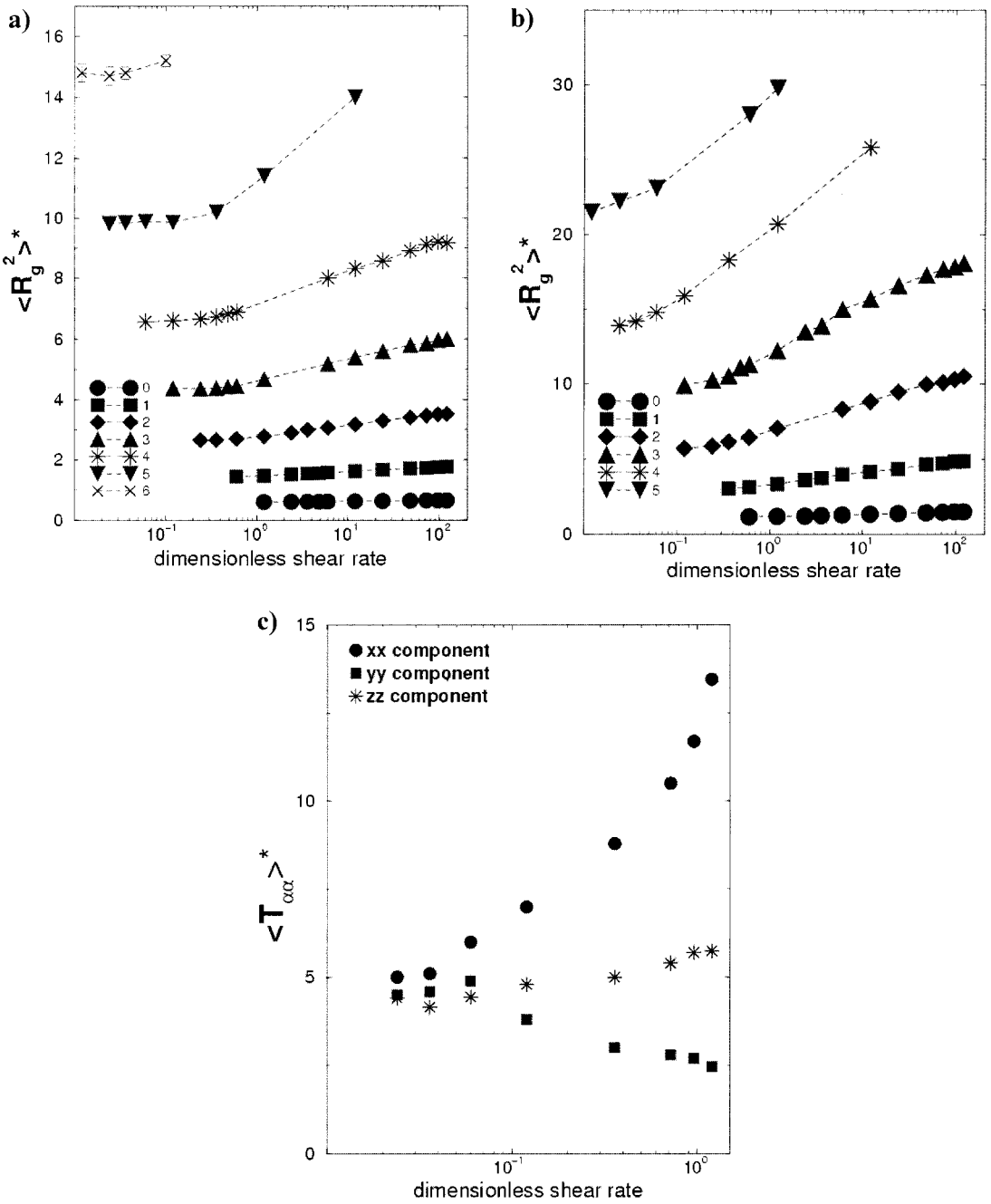

Figure 4. Dependence of the dimensionless mean-squared radius of gyration on dimensionless shear rate for (a) a model A and (b) a model B dendrimer with the number of generations, g, ranging from 0 to 6. All simulations are performed in the presence of hydrodynamic interactions ($h^* = 0.25$). The onset of the visible increase in the radius of gyration is close to the onset of the shear-thinning of the corresponding intrinsic viscosities. Dependence of the three different diagonal components of the mean gyration tensor on the magnitude of shear flow is shown in part c for model B and generation $g = 4$.

Mansfield and Klushin[14] calculated the intrinsic viscosity for PAMAM dendrimers using the Lescanec–Muthukumar model.[8] In these calculations, the excluded volume of the monomer treated as a rigid sphere is equated to its hydrodynamic volume. The results of MC simulations[18] showed that the maximum in the dependence of intrinsic viscosity vs g is observed only when the characteristic size of the excluded volume interactions of monomer is smaller than its hydrodynamic radius. Within the simulations in this manuscript, the characteristic excluded size of the bead is 0.5σ where σ is the Lennard–Jones parameter. The ratio Ω of excluded size to hydrodynamic radius a is equal to 1.56 when h^* is 0.25 and is equal to 0.89 when h^* is 0.44. As seen in Figure 3, the effect of decreasing the value of Ω tends to shift the peak in the $[\tilde{\eta}]_0$ vs g plots toward smaller generations. On the other hand, the free draining (i.e., $h^* = 0$) situation corresponds to the limiting case of $\Omega \rightarrow \infty$ and does not illustrate a maximum within Figure 3.

The occurrence of maxima within the $[\tilde{\eta}]_0$ vs g plots when $\Omega > 1$ can be understood in terms of an argument given by Chen and Cai[18] within their MC simulations of dendrimers. They propose the attractive portion of the Lennard–Jones potential compensates part of the repulsion between the beads of the dendrimer thereby

making 0.5σ an overestimation of the characteristic excluded size of a bead to be used in the calculation of Ω.

B. Radius of Gyration. The mean-squared radius of gyration, $\langle R_g^2\rangle^*$, as a function of shear rate for dendrimers of varying generation g, is shown in parts a (model A) and b (model B) of Figure 4. $\langle R_g^2\rangle^*$ slightly increases with increasing shear rate for smaller dendrimers but increases much more sharply at some critical shear rate for dendrimers with 4−6 generations. This critical shear rate also denotes the onset of shear-thinning as depicted in parts a and b of Figure 2. At a given shear rate, the relative increase in radius of gyration is higher for model B dendrimers.

The three diagonal terms of the gyration tensor $\langle T_{\alpha\alpha}\rangle^*$, with $\alpha = x$, y, and z, characterize the average dimensions of the dendrimer in the three directions where the x direction is the flow direction. These components appear in Figure 4c for the $g = 4$ model B dendrimer. The xx component reveals the dendrimer is stretched more and more along the flow direction as the shear rate is increased. At the same time, the yy component decreases with shear with a slight increase in the zz component.

Figure 5a compares the effect of shear on two dendrimers and a linear analogue where all three molecules have approximately the same value of $\langle R_g^2\rangle^*$ in the absence of shear flow. One dendrimer is a $g = 5$ model A, the other dendrimer is a $g = 3$ model B, and the linear chain has flexible valence angles, excluded volume, and hydrodynamic interactions. With increasing shear rate, the linear chain is seen to pass through a maximum at moderate shear rates due to the development of chain foldings.[24] In contrast, $\langle R_g^2\rangle^*$ for the model A dendrimer does not change until dimensionless shear rates of approximately 0.1 whereas $\langle R_g^2\rangle^*$ for the model B dendrimer grows steadily from the application of shear flow.

The affect of hydrodynamic interactions on the shear behavior of $\langle R_g^2\rangle^*$ for a $g = 6$ model A dendrimer and a $g = 5$ model B dendrimer is shown on Figure 5b. At low shear rates, Newtonian behavior is observed with the nondraining $\langle R_g^2\rangle^*$ values very close to their free-draining analogues as expected. At higher shear rates, $\langle R_g^2\rangle^*$ for the nondraining and free-draining model A cases remain very similar to the nondraining model B dendrimer illustrating a much weaker shear rate dependence of $\langle R_g^2\rangle^*$ relative to the free-draining model B dendrimer. Noticeable stretching should occur when the magnitude of the shear rate, $\dot\gamma$, is inversely proportional to the characteristic relaxation time of the whole chain.[25] For the Rouse model this relaxation time is proportional to N^2. For models with HI, the chain relaxation time scales as $N^{3/2}$ revealing why the stretching of these chains occurs at higher magnitudes of $\dot\gamma$. The dependence of the mean-squared radius of gyration at zero shear, $\langle R_g^2\rangle_0^*$, on molecular weight and generation number is illustrated in parts a and b of Figure 6 for model A and model B dendrimers. For sufficiently long linear polymer chains and under the influence of hydrodynamic and excluded volume interactions, $\langle R_g^2\rangle_0^* \sim N$ as revealed by the open symbols within Figure 6a. This does not come as a surprise as the Lennard−Jones parameters were chosen to reproduce Θ-conditions for linear chains.[22]

Deviation from this scaling behavior for the shorter chains ($N < 30$) in Figure 6a) shows that they are not long enough to follow the universal scaling dependence. For the dendrimers, $\langle R_g^2\rangle_0^* \sim N$ for the first two model A and model B generations. Generations 3−6 for both model A and model B dendrimers reveal $\langle R_g^2\rangle_0^* \sim N^{0.62}$ which is very similar to the findings of Mansfield and Klushin on a Monte Carlo investigation of PAMAM where $\langle R_g^2\rangle_0^* \sim N^{0.60}$. These data are also plotted in Figure 6a. In general, this behavior is not expected to

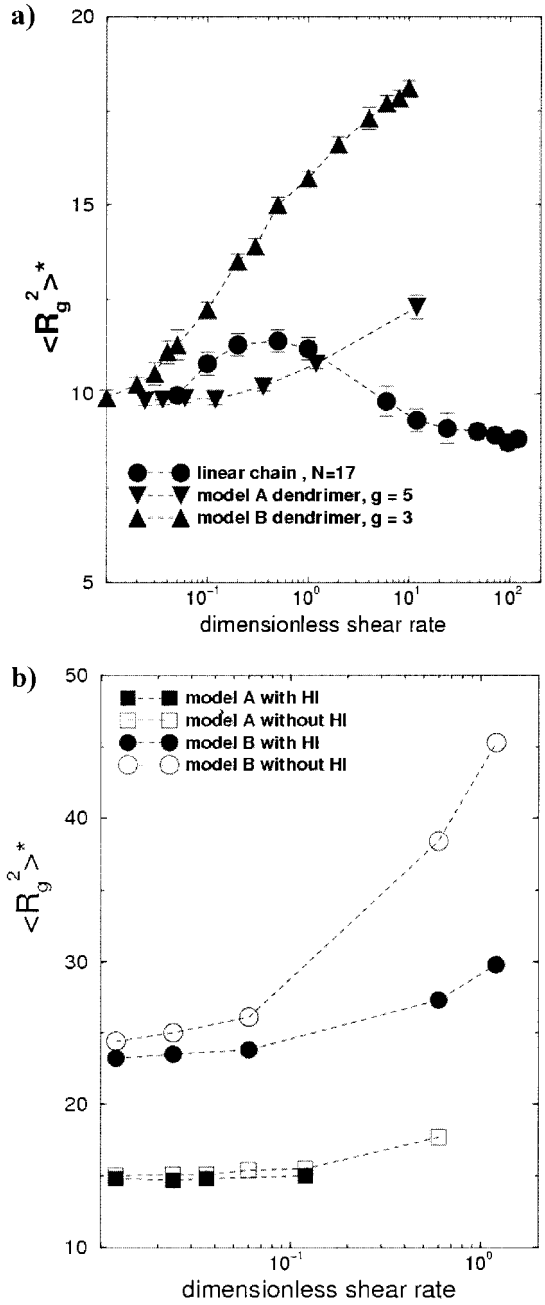

Figure 5. (a) Dependence of the dimensionless mean-squared radius of gyration on dimensionless shear rate for a model A, $g = 5$ (triangles down) and a model B, $g = 3$ (triangles up) dendrimer in the presence of hydrodynamic interactions ($h^* = 0.25$). The linear chain is simulated with HI ($h^* = 0.25$), excluded volume interactions in addition to valence angle and torsional angle potentials (closed circles). (b) Dependence of the dimensionless mean-squared radius of gyration on dimensionless shear rate for a model A, $g = 3$ and a model B, $g = 5$ dendrimer with HI ($h^* = 0.25$; closed symbols) and without HI ($h^* = 0$; open symbols). Inclusion of the HI affords a weaker shear rate dependence of the mean-squared radius of gyration for both models.

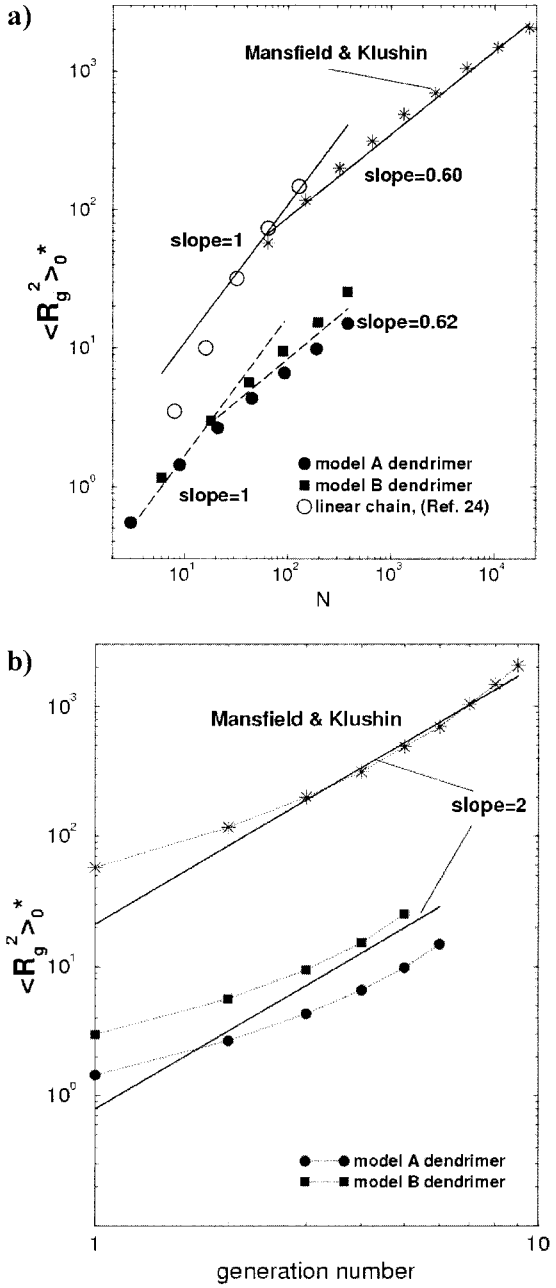

Figure 6. (a) Dependence of the dimensionless mean-squared radius of gyration in the absence of shear on number of monomers N. Filled symbols represent results from simulations performed in the presence of hydrodynamic interactions ($h^* = 0.25$). BD simulation results in the presence of hydrodynamic interactions ($h^* = 0.25$) for a linear chain within a Θ solvent are shown by open spheres. MC results from PAMAM dendrimer simulations[14] are also reported. The slope of 0.62 for models A and B is very close to that for PAMAM dendrimer from Reference 14. (b) Dependence of the dimensionless mean-squared radius of gyration in the absence of shear on generation number g. All simulations are performed in the presence of hydrodynamic interactions ($h^* = 0.25$). MC results from simulation of PAMAM dendrimers from ref 14 are also reported. The slope of 2 for models A and B is very close to that for a PAMAM dendrimer from ref 14.

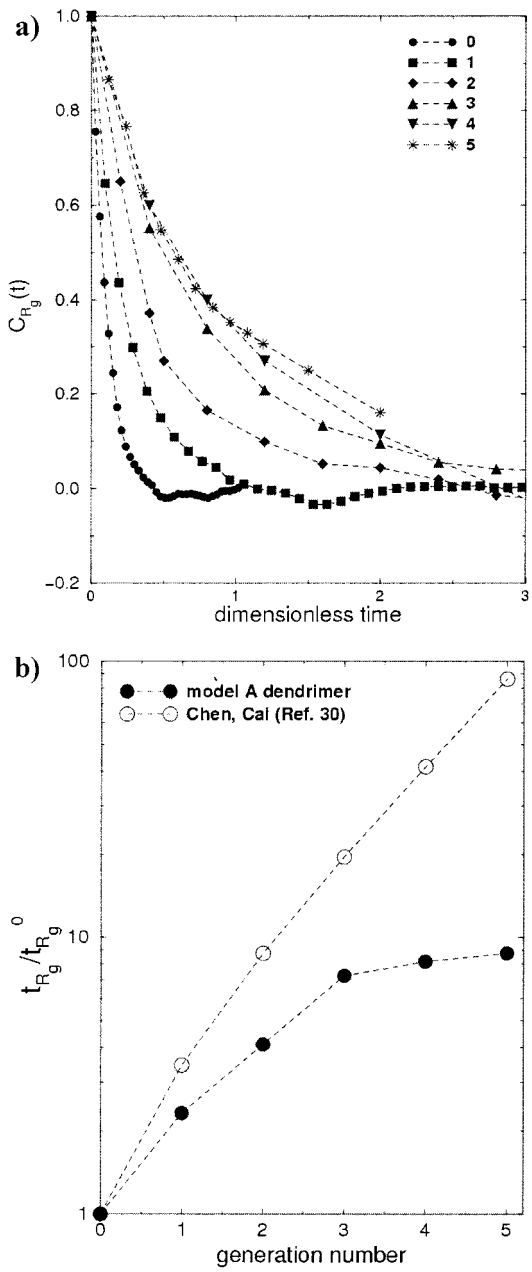

Figure 7. (a) Autocorrelation functions of the radius of gyration (eq 8) of a model A dendrimer for different generation numbers, g, ranging from 0 to 6. All simulations are performed in the presence of hydrodynamic interactions ($h^* = 0.25$). (b) Dependence of characteristic relaxation times normalized to that for the dendrimer of generation 0 for model A in the present simulations (closed circles) and results of MC simulations performed by Chen and Cai[28] (open circles).

be valid at higher generations even for ideal dendrimers where excluded volume interactions are not considered.[27] In this case $\langle R_g^2\rangle_0^* \sim g$ and $N \sim 2^g$ indicating that $\langle R_g^2\rangle_0^* \sim \log N$.

Figure 6b analyses the dependence of $\langle R_g^2\rangle_0^*$ in terms of the generation number g. As compared to ideal dendrimers the results of the present simulations show that the incorporation of excluded volume effects leads to the stronger dependence, $\langle R_g^2\rangle_0^* \sim g^2$. The quadratic behavior is observed for model A and model B dendrimers starting at the third or fourth generation which is again in good agreement with the work of Mansfield and Klushin.[14]

C. Autocorrelation Function of Radius of Gyration. Figure 7a depicts the normalized autocorrelation function of the squared radius of gyration, $C_{R_g}(t)$, for the model A dendrimer calculated in the absence of shear. $C_{R_g}(t)$ is observed to decay the quickest for the lower generations with the higher generations decaying the slowest with the curves for generations 4 and 5 overlapping up to nearly the first unit of dimensionless time.

Figure 7b plots the values of a characteristic relaxation time, t_{R_g}, for different generation numbers of the model A dendrimer (filled symbols) where t_{R_g} is defined as the condition where $C_{R_g}(t_{R_g}) = e^{-1}$ and $t^0{}_{R_g}$ is the characteristic time for the zeroth generation model A dendrimer. As expected from the data in Figure 7b, the dependence of t_{R_g} on generations 3−5 is very weak. Chen and Cai[28] calculated t_{R_g} using Monte Carlo simulations to carry out the calculation of the hydrodynamic tensor, eigenvalues of the effective force matrix and characteristic relaxation times for a similar dendrimer model using preaveraged hydrodynamic interactions and excluded-volume repulsions. They performed these calculations at different values of the hydrodynamic radius and their values of relaxation times using $a = 0.316l$ are plotted in Figure 7b as open symbols. Relative to the values from the present investigation using $a = 0.257l$ the Chen and Cai data reveal a much stronger dependence of relaxation times on generation number. This difference may be due to fluctuations of the hydrodynamic interactions which are not considered when using preaveraged hydrodynamic interactions and naturally take place in the present Brownian dynamics simulations.

D. Translational Mobility and Hydrodynamic Radius. The translational mobility of the model A and model B dendrimers has been studied by the mean-square translational displacement of their respective center of masses (COM). These dependencies are almost linear functions of time in all region of times covered by these simulations and hence data are not shown. The COM diffusion coefficient for each dendrimer is extracted from these data using the Einstein relationship $\langle \Delta r^2(t) \rangle = 6D_{com}t$. For nondraining polymers, the hydrodynamic radius, R_h, of the whole molecule is possible to determine from the diffusion coefficient using the simple Stokes relation

$$D_{com} = kT/6\pi\eta_s R_h \tag{10a}$$

where η_s is the viscosity of the solvent. It is also possible to calculate the hydrodynamic radius as[29]

$$R_h{}^{-1*} = \frac{1}{N^2}\left\langle \sum_{i,j\neq i}^{N} \frac{1}{|\vec{r}_{ij}|^*} \right\rangle \tag{10b}$$

where $|\vec{r}_{ij}|^*$ represents the separation between two beads and the angular brackets denote an average over the phase trajectory. Finally, the hydrodynamic radius for an effective sphere representing the whole dendrimer can be calculated from its zero-shear intrinsic viscosity according to[25]

$$[\tilde{\eta}]^* = \frac{10\pi}{3N} R_h{}^{3*} \tag{10c}$$

Values for R_h computed from these different approaches are compared in Figure 8 along with the average radius of gyration, $R_g^* = \sqrt{\langle R_g{}^2 \rangle_0^*}$.

It is seen that R_g^* is slightly larger than the hydrodynamic radii calculated from the diffusion coefficient (eq 10a) and from the intrinsic viscosity (eq 10c) which themselves are very similar. The hydrodynamic radius calculated from the preaveraged approach given by eq 10b is slightly larger especially at low generation numbers. This again implies that the fluctuations of the HI which are not taken into account by a preaveraging approach play an important role.

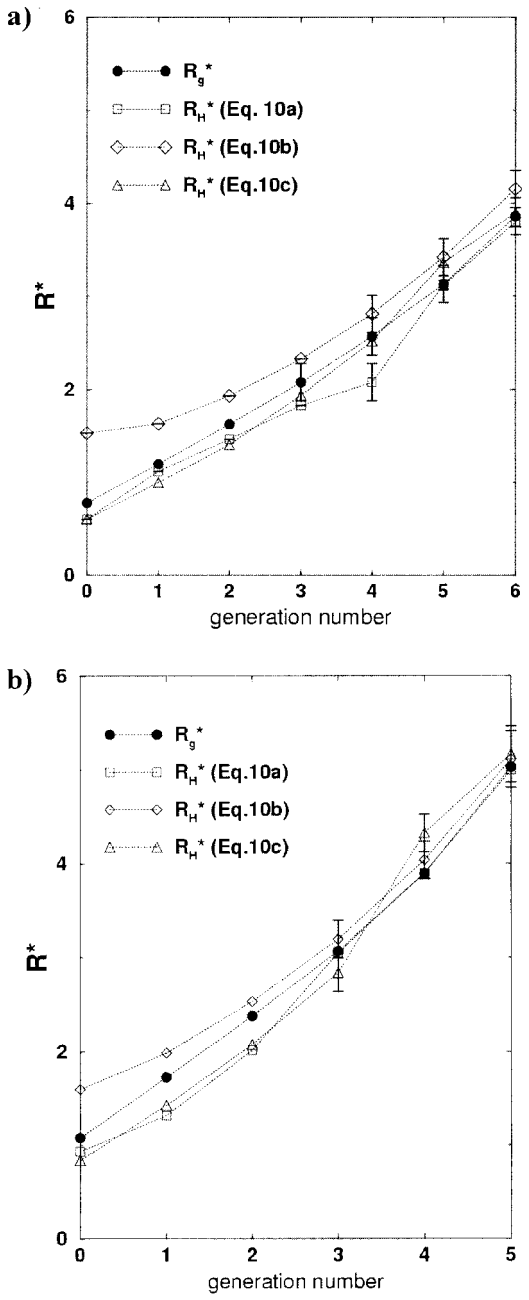

Figure 8. Dependence of the dimensionless average radius of gyration and hydrodynamic radii defined in eq 10a−c on generation number for (a) a model A and (b) a model B dendrimer in the absence of shear. All simulations are performed in the presence of hydrodynamic interactions ($h^* = 0.25$). The hydrodynamic radius calculated in a preaveraged approach (eq 10b) is higher than R_g^* and R_H^* obtained via eq 10a and eq 10c.

E. Radial Density Profiles. Parts a and b of Figure 9 display the average number density of monomers (in the absence of shear) in concentric shells about the center of mass which is taken as the origin. They are normalized in such a way that the volume integral is equal to the total number of monomers. In all the dendrimers, a core region with high density is observed near the origin. For small generation numbers, the density monotonically decreases with increasing distance from the origin. Increasing the generation number leads to shallow minima[9] followed by a shoulder of

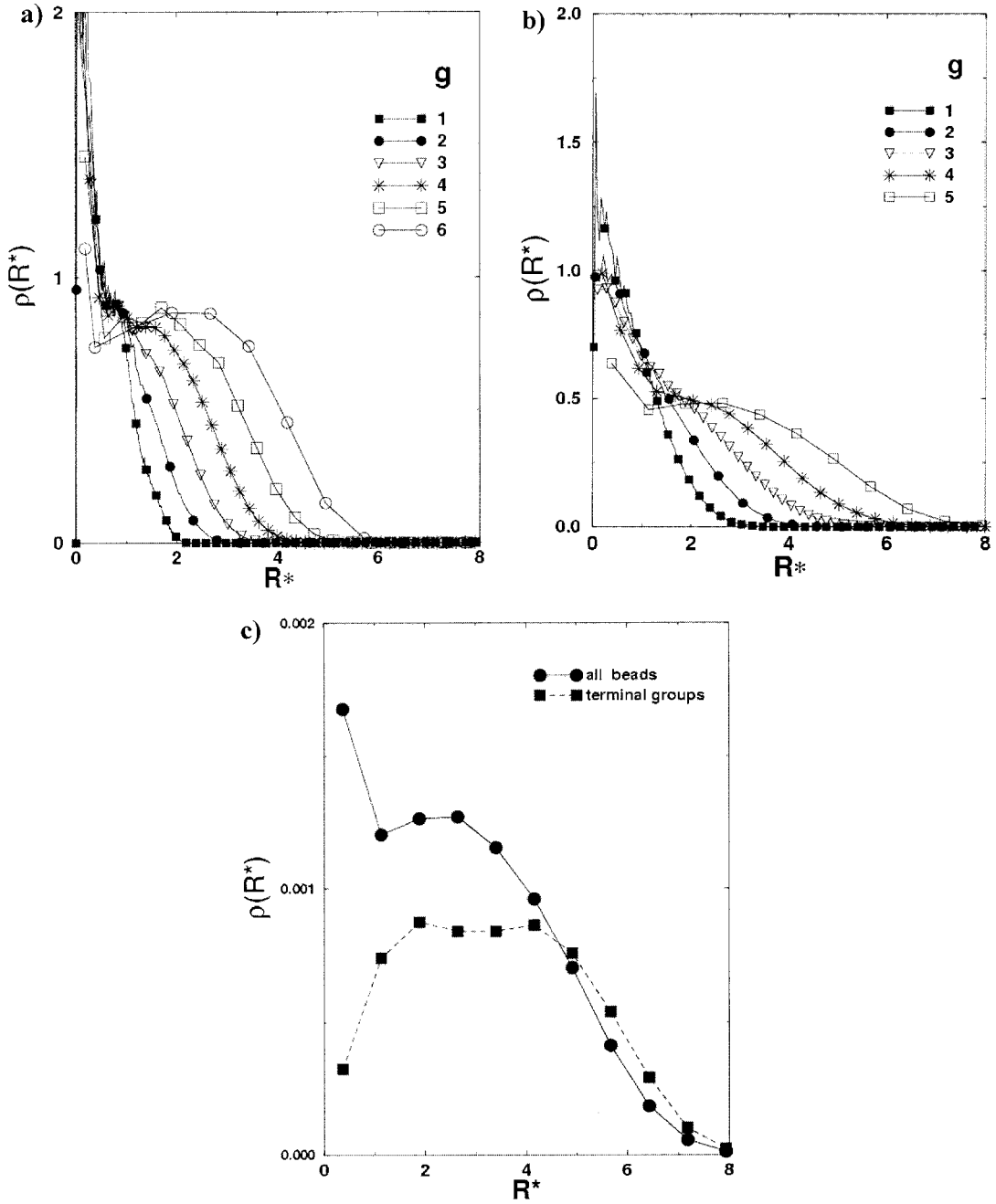

Figure 9. Dependence of the radial distribution function of monomers on the distance from the center of mass for (a) a model A and (b) a model B dendrimer in the absence of shear. All simulations are performed in the presence of hydrodynamic interactions ($h^* = 0.25$). For large generation numbers, $g > 5$, these dependences pass through a relative minimum before first increasing and finally decreasing again. (c) The distribution function of the terminal groups only for the model B $g = 5$ dendrimer is shown in comparison with the distribution function of all segments for the same dendrimer.

nearly constant density inside the dendrimer. For dendrimers of $g = 5$ and $g = 6$ each plateau is observed when distance R^* from the core is $1 \leq R^* \leq 3$.

Figure 9c gives the distribution function of the terminal groups for a model B $g = 5$ dendrimer and the distribution function for all segments for the same dendrimer where the area beneath both curves has been set to unity. It is clear that segments belonging to the last generation are dispersed throughout the whole molecule except in the region near the core which is in agreement with previous simulations [8,9,11]. The dimensionless radius of gyration, $R^*_{g,w}$, generated from the distribution function for all segments is 4.9 ± 0.2 where the dimensionless radius of gyration, $R^*_{g,t}$, calculated using only the terminal groups is 5.4 ± 0.2. The relative difference

$$\Delta = \frac{R^*_{g,t} - R^*_{g,w}}{R^*_{g,w}} \tag{11}$$

is equal to $\Delta \cong 0.10$. Recently Topp et al.[30] published the results of small-angle neutron scattering experiments on PAMAM dendrimers using deuterium labeling and scattering contrast variation. For generation 7 PAMAM, the radius of gyration of deuterated terminal units, $R_{g,t} = 39.3 \pm 1.0$ Å, was observed to be signifi-

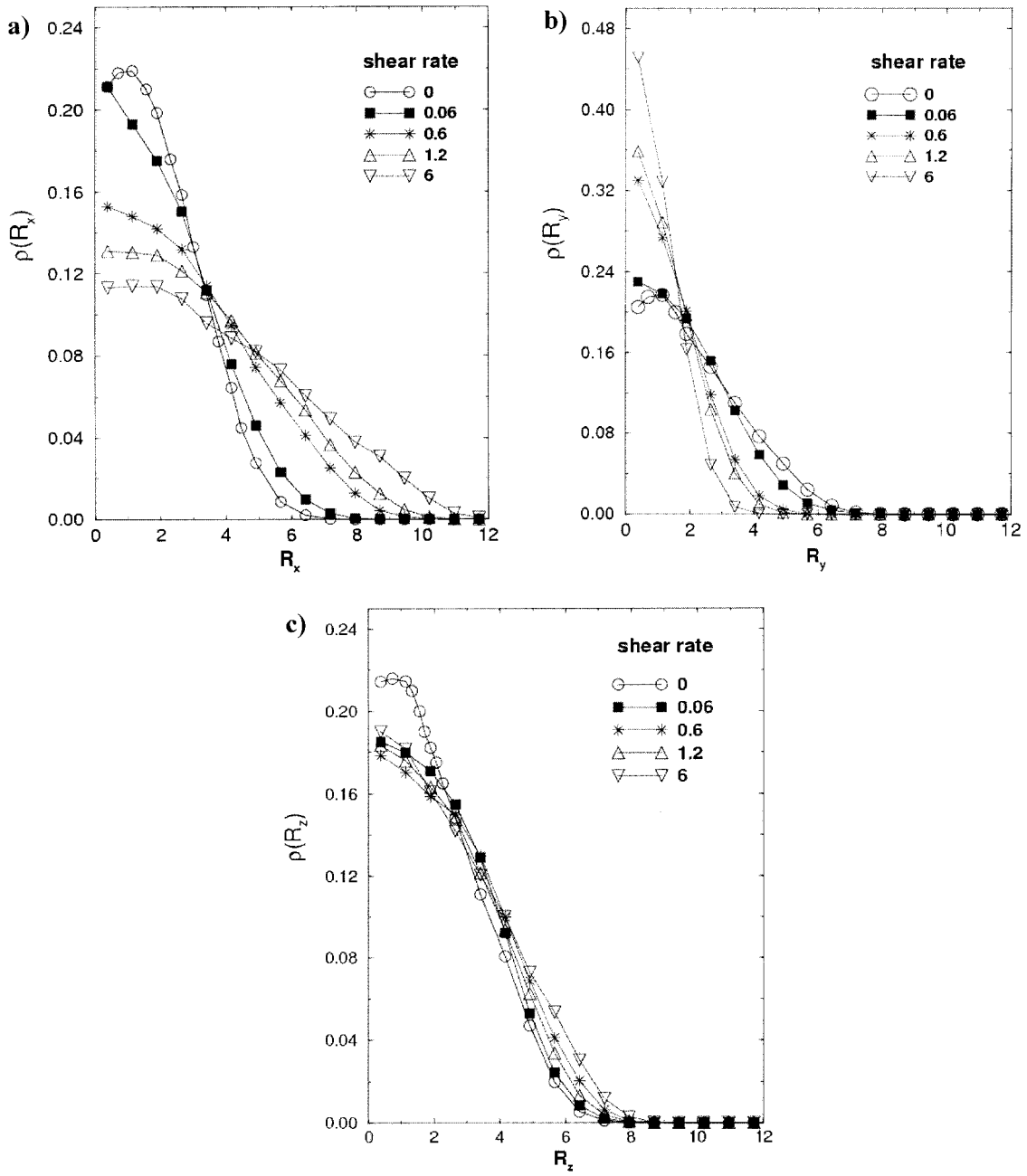

Figure 10. Dependence of the linear distribution functions of monomers on the distance from the center of mass for a model B, $g = 5$ dendrimer under the influence of shear flow along (a) the x axis (b) the y axis and (c) the z axis. All simulations are performed in the presence of hydrodynamic interactions ($h^* = 0.25$). As the magnitude of the flow increases, the peak in the distribution of monomers along the x axis lowers with a corresponding broadening of the distribution. On the contrary, the distribution of monomers along the y axis become sharper as the flow increases. The distribution of monomers along the z axis is relatively unaffected by increasing flow rate.

cantly larger than that for the whole dendrimer, $R_{g,w} = 34.4 \pm 0.2$. The relative difference Δ from (11) is in very good agreement with the neutron scattering experiments[30] which give $\Delta \cong 0.14$. The fact that $R^*_{g,t}$ is larger than $R^*_{g,w}$ could lead one to infer that the terminal groups are located on the periphery of the dendrimer. Figure 9c reveals that this is not the case and indicates that care must be taken when using the relative magnitudes of $R^*_{g,t}$ and $R^*_{g,w}$ to ascertain how the terminal groups are distributed within a dendrimer.

In parts a−c of Figure 10 we plot the linear density profiles (normalized to unity) for the largest system studied in this paper (model B of generation $g = 5$) under the influence of shear flow. In this case, the density is calculated along three different axes separately because the dendrimer is no longer spherically symmetric. In the absence of shear, all three linear densities are similar in shape with a peak at small values of R_x, R_y, and R_z. Under the influence of shear the dendrimer elongates in the x direction which flattens the corresponding distribution function (Figure 10a). The squeezing in the perpendicular direction leads to the increase of the monomer density around center of mass in this direction (Figure 10b). The linear distribution in the z direction is not strongly affected by the shear flow (Figure 10c).

IV. Conclusions

BD computer simulations of model nondraining dendritic polymers with and without spacers have been performed under the influence of shear flow. A freely jointed model of dendrimer with rigid bonds, excluded volume, and HI interactions is used. Up to 6 generations of dendrimers are simulated. The major conclusions are:

(1) Shear-thinning is observed for both models. The onset of shear-thinning starts at a higher magnitude of shear flow as compared to linear analogues of nondraining chains with the same molecular weight.

(2) The maximum in the dependence of zero-shear rate viscosity on the generation number is observed for nondraining dendrimers and is located at $g \sim 4$. The peak in the intrinsic viscosity is only observed when HI are invoked. Increasing the strength of HI (dimensionless parameter h^*) leads to an even more pronounced maximum shifted to smaller generations. Fluctuations of HI, explicitly taken into account in the present simulations, are very important: the hydrodynamic radius calculated from the coefficient of translational diffusion is very close to that calculated from the zero-shear viscosity and to the average radius of gyration of the dendrimer. At the same time, a preaveraged approach leads to a higher value for the hydrodynamic radius.

(3) Shear flow leads to a monotonical increase in the radius of gyration of dendrimers in contrast to a linear chain where chain foldings were observed.

(4) Characteristic relaxation times for the autocorrelation function of the radius of gyration increase with increasing generation numbers much more slowly than predicted by a MC simulation[28] of the model with preaveraged hydrodynamic interactions.

(5) A radius of gyration based only on terminal units that is larger than a radius of gyration based on all monomers of a dendrimer does not automatically imply the terminal units are located on the periphery of the dendrimer.

Acknowledgment. The authors acknowledge the EPSRC for financial support of this study (GR/L79229). This work has been computed on the Leeds University HPC Modeling Facility partially funded under the 1997 Joint Research Equipment Initiative of the Research and Funding Councils. A.V.L. acknowledges partial travel assistance from the Russian Foundation for Basic Research (RFBR grant 9903-33314a). Stimulating discussions with V. Pryamitsyn and L. Klushin are gratefully acknowledged.

References and Notes

(1) Buhleiler, E.; Wehner, W.; Vögtle, F. *Synthesis* **1978**, 155.
(2) Tomalia, D. A.; Baker, H.; Dewald, J.; Hall, M.; Kallos, G.; Martin, S.; Roeck, J.; Ryder, J.; Smith, P. *Polym. J.* **1985**, *17*, 117.
(3) Fréchet, J. M. J.; Hawker, C. J.; Wooley, K. L. *J. Macromol. Sci.—Pure Appl. Chem.* **1994**, *A31*, 1627.
(4) Fréchet, J. M. J. *Science* **1994**, *263*, 1710.
(5) Tomalia, D. A.; Naylor, A. M.; Goddard, W. A., III. *Angew. Chem., Int. Ed.* **1995**, *29*, 138.
(6) de Gennes, P. J.; Hervet, H. *J. Phys. Lett. Fr.* **1983**, *44*, L351.
(7) Naylor, A. M.; Goddard, W. A., III; Kiefer, G. E.; Tomalia, D. A. *J. Am. Chem. Soc.* **1989**, *111*, 2339.
(8) Lescanec, R. L.; Muthukumar, M. *Macromolecules* **1990**, *23*, 2280.
(9) Mansfield, M. L.; Klushin, L. I. *Macromolecules* **1993**, *26*, 4262.
(10) Lue, L.; Prausnitz, J. M. *Macromolecules* **1997**, *30*, 6650.
(11) Murat, M.; Grest, G. *Macromolecules* **1996**, *29*, 1278.
(12) Mazo, M. A.; Sheiko, S. S.; Zhilin, P. A.; Gusarova, E. B.; Balabaev, N. K. *Izv. Akad. Nauk, Ser. Phys.* (in Russian) **1998**, *62*, 1098.
(13) Okumoto, M.; Tasaka, Y.; Nakamura, Y.; Norisuye, T. *Macromolecules* **1999**, *32*, 7430.
(14) Mansfield, M. L.; Klushin, L. I. *J. Phys. Chem.* **1992**, *96*, 3994.
(15) Fixman, M. *J. Chem. Phys.* **1983**, *78*, 1588.
(16) Aerts, J. *Comput. Theor. Polym. Sci.* **1998**, *2*, 49.
(17) Widmann, A. H.; Davies, G. R. *Comput. Theor. Polym. Sci.* **1998**, *8*, 191.
(18) Cai, C.; Chen, Z. Y. *Macromolecules* **1998**, *31*, 6393.
(19) Uppuluri, S.; Keinath, S. E.; Tomalia, D. A.; Dvornic, P. R. *Macromolecules* **1998**, *31*, 4498.
(20) Ermak, D. L.; McCammon, J. A. *J. Chem. Phys.* **1978**, *69*, 1352.
(21) Ryckaert, J.-P.; Bellemans, A. *Chem. Phys. Lett.* **1975**, *30*, 123.
(22) Rey, A.; Freire, J. J.; García de la Torre, J. *Macromolecules* **1987**, *20*, 2385.
(23) Rotne, J.; Prager, S. *J. Chem. Phys.* **1969**, *50*, 4831.
(24) Lyulin, A. V.; Adolf, D. B.; Davies, G. R. *J. Chem. Phys.* **1999**, *111*, 758.
(25) Doi, M.; Edwards, S. F. *The Theory of Polymer Dynamics*; Oxford University Press: Oxford, U.K., 1986.
(26) Tomalia, D. A.; Naylor, A. M.; Goddard, W. A., III. *Angew. Chem.* **1990**, *102*, 119.
(27) Chen, Z. Y.; Cui, S.-M. *Macromolecules* **1996**, *29*, 7943.
(28) Chen, Z. Y.; Cai, C. *Macromolecules* **1999**, *32*, 5432.
(29) Grosberg, A. Yu., Khokhlov, A. R. *Statistical Physics of Macromolecules*; AIP Press: Woodbury, NY, 1994.
(30) Topp, A.; Bauer, B. J.; Klimash, J. W.; Spindler, R.; Tomalia, D. A.; Amis, E. J. *Macromolecules* **1999**, *32*, 7226.

MA992128A